Supplementary Information (SI) for Nanoscale.

Supplementary Information for

Hydration Shell Water Surrounding Citrate-Stabilised Gold Nanoparticles

Taritra Mukherjee,[a,b] Elspeth K. Smith,[c] Marialore Sulpizi[c] and Martin Rabe[a]

a. Department of Interface Chemistry and Surface Engineering, Max Planck Institute for Sustainable Materials, Max-Planck-Straße 1, 40237 Düsseldorf, Germany
b. Fakultät für Chemie und Biochemie, Ruhr-Universität Bochum, Universitätstraße 150, 44801 Bochum, Germany
c. Fakultät für Physik und Astronomie, Ruhr-Universität Bochum, Universitätstraße 150, 44801 Bochum, Germany

Table of Contents

1. Dilution table

Table S1.

NP Series	Nominal radius$^{(A)}$ (m)	Concentration in supplied samples$^{(B)}$ (mL^{-1})	Dilution factor for 100% sample$^{(C)}$	Total nominal surface area in 100% sample$^{(D)}$ (m^2/mL)
NP10	5×10^{-9}	5.46×10^{12}	0.2289375	3.927×10^{-4}
NP30	1.5×10^{-8}	1.84×10^{11}	0.1509665	7.854×10^{-5}
NP50	2.5×10^{-8}	4.37×10^{10}	0.2288335	7.854×10^{-5}

(A) $Nominal\ radius\ = r$

(B) $Concentration\ = n$, provided by the supplier, Nanopartz Inc.

(C) $Dilution\ factor = \frac{Volume\ of\ original\ supplied\ NP\ dispersion}{Total\ volume\ of\ 100\%\ sample} = f$

(D) $NP\ surface\ area\ in\ 100\%\ sample = 4\pi r^2 nf$

2. Amount of citrate in supplied samples

According to the information sheet provided by the supplier, the citrate concentrations in the original (supplied) stock dispersions of NP10, NP30 and NP50 were 3 mM, 5 mM and 3 mM, respectively.

3. UV-visible spectra

The UV-visible spectra (**Figure S1**) were recorded with water as the background, for all the originally received samples, the NP-containing samples in the dilution series and the centrifuged-out supernatant liquids, i.e., the dispersing media. The path length was 1 cm, the slit width used, was 1 nm and the absorbance values were recorded for 0.52 s at each data point.

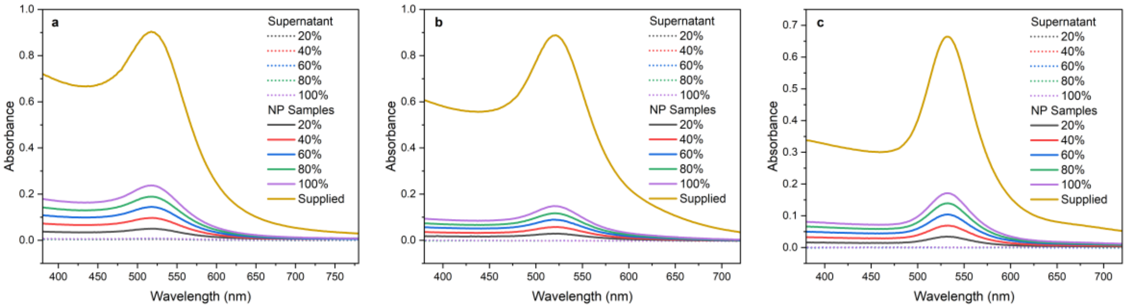

Figure S1. UV-Visible spectra for the NP samples (solid lines) and centrifuged-out dispersing media (dotted lines) for a. NP10, b. NP30 and c. NP50 series.

The wavelengths of maximum absorption for NP10, NP30 and NP50 are around 518 nm, 522 nm and 531 nm respectively. The negligible absorbance observed for the supernatant liquids attest to adequate centrifugation.

4. Light scattering measurements

Dynamic and electrophoretic light scattering measurements were carried out on the supplied NP samples and the dilution series for the NPs, using Anton Paar Litesizer 500 with the help of its associated Kalliope software. However, no reproducible data were obtained for NP10 series. The following table describes the twice-measured hydrodynamic diameter and zeta potential values for the NP30 and NP50 series. The absolute values of zeta potential are all quite significantly greater than 25 mV, indicating that the dispersions were stable.

Table S2.

NP Series	*Sample*	*Hydrodynamic diameter (nm)*	*Polydispersity index in %*	*Zeta potential (mV)*	*Standard deviation (mV)*
NP30	20%	59.62	28.20	-72.21	4.21
		57.94	27.40	-72.40	3.07
	40%	47.32	27.14	-83.32	3.51
		51.34	26.57	-77.14	3.10
	60%	43.87	26.36	-71.95	1.82
		47.80	26.65	-70.51	1.98
	80%	40.41	25.57	-81.47	1.69
		42.18	25.69	-81.64	2.56
	100%	46.90	26.89	-81.17	2.12
		44.64	27.00	-82.64	1.86
	Supplied	37.36	25.97	-70.17	1.32
		36.97	25.77	-71.60	2.22
NP50	20%	81.12	22.10	-80.44	2.00
		78.05	20.12	-81.11	3.20
	40%	73.67	18.00	-76.16	3.04
		74.61	17.74	-78.08	3.78
	60%	73.04	17.91	-78.23	2.26
		72.16	17.88	-76.69	3.70
	80%	71.51	16.01	-80.29	3.38
		71.37	16.50	-78.50	2.70
	100%	70.93	17.67	-78.08	2.56
		70.52	17.22	-77.41	1.88
	Supplied	70.21	15.70	-74.36	2.60
		69.02	16.82	-72.56	1.79

5. Raw Raman spectra

The Raman spectra of the samples are presented in **Figure S2**, as measured, without any correction.

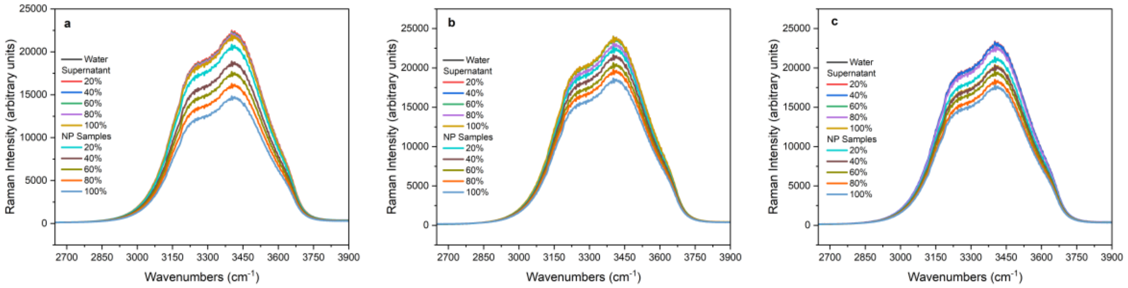

Figure S2. The raw Raman spectra for water used for dilution, dispersing media (supernatant) and NP-containing samples for a. NP10, b. NP30 and c. NP50 series.

6. Gaussian fitting parameters used to prepare Figure 2

Table S3.

Series	Samples	Spectra	Gaussian Components	Area/Total Area	Position	FWHM
NP10	20%	Bulk	FP1	0.55067	3258.818	272.6757
			FP2	0.31304	3443.737	177.1226
			FP3	0.13082	3586.206	160.4836
		Solute-correlated	FP1	0.48212	3227.239	255.3829
			FP2	0.40344	3421.72	187.5788
			FP3	0.11279	3574.502	138.9488
	40%	Bulk	FP1	0.55057	3258.449	272.6137
			FP2	0.31351	3443.488	177.2027
			FP3	0.13045	3586.049	160.2626
		Solute-correlated	FP1	0.52425	3270.587	296.7417
			FP2	0.33532	3440.584	184.8696
			FP3	0.13424	3583.303	151.4684
	60%	Bulk	FP1	0.55073	3258.39	272.7521
			FP2	0.31293	3443.267	177.0698
			FP3	0.13088	3585.734	160.4016
		Solute-correlated	FP1	0.50631	3288.389	299.9842
			FP2	0.33136	3447.643	188.6518
			FP3	0.14467	3589.152	157.8255
	80%	Bulk	FP1	0.55014	3258.213	272.5546
			FP2	0.31439	3443.322	177.4631
			FP3	0.13011	3586	160.1449
		Solute-correlated	FP1	0.4649	3294.997	286.0572
			FP2	0.30004	3440.066	169.1934
			FP3	0.21324	3576.293	167.7102
	100%	Bulk	FP1	0.55061	3258.228	272.7623
			FP2	0.31392	3443.328	177.3593
			FP3	0.13003	3585.974	160.0765
			FP1	0.4506	3313.69	282.0038

		Solute-correlated	FP2	0.30047	3441.691	171.7995
			FP3	0.22481	3578.294	169.8777
NP30	20%	Bulk	FP1	0.55044	3258.425	272.4639
			FP2	0.31373	3443.511	177.1388
			FP3	0.13044	3586.08	160.161
		Solute-correlated	FP1	0.4969	3244.412	268.1064
			FP2	0.34434	3426.642	182.6415
			FP3	0.15353	3570.003	167.3441
	40%	Bulk	FP1	0.54967	3258.193	272.3385
			FP2	0.31483	3443.408	177.5365
			FP3	0.13013	3586.09	160.2443
		Solute-correlated	FP1	0.53652	3264.897	281.6447
			FP2	0.31112	3440.939	172.6832
			FP3	0.14762	3581.644	151.6628
	60%	Bulk	FP1	0.54977	3258.173	272.4003
			FP2	0.31466	3443.411	177.4668
			FP3	0.13011	3586.1	160.1885
		Solute-correlated	FP1	0.52172	3273.055	289.9797
			FP2	0.30006	3438.885	174.2334
			FP3	0.16728	3578.886	160.9548
	80%	Bulk	FP1	0.55029	3258.294	272.5631
			FP2	0.31416	3443.443	177.3164
			FP3	0.13016	3586.086	160.1007
		Solute-correlated	FP1	0.47649	3269.219	277.7132
			FP2	0.31518	3431.621	174.4936
			FP3	0.20095	3570.009	170.9117
	100%	Bulk	FP1	0.55032	3258.183	272.5861
			FP2	0.31376	3443.246	177.2654
			FP3	0.1305	3585.814	160.3029
		Solute-correlated	FP1	0.51689	3297.996	299.9896
			FP2	0.30052	3449.996	178.6057
			FP3	0.16512	3587.31	158.335
NP50	20%	Bulk	FP1	0.55097	3258.205	272.9311
			FP2	0.31309	3443.237	177.2306
			FP3	0.13035	3585.798	160.301
		Solute-correlated	FP1	0.48699	3235.193	262.7842
			FP2	0.38956	3427.314	191.1886
			FP3	0.11841	3578.926	149.6016
	40%	Bulk	FP1	0.55122	3258.199	273.0721
			FP2	0.31243	3443.117	177.1072
			FP3	0.13068	3585.628	160.4556
		Solute-correlated	FP1	0.48483	3245.22	265.0505
			FP2	0.41704	3439.609	200.1602
			FP3	0.09527	3590.802	138.6315
	60%	Bulk	FP1	0.5511	3258.118	272.9542
			FP2	0.31319	3443.156	177.2541
			FP3	0.13023	3585.703	160.1965

		Solute-correlated	FP1	0.46308	3243.113	279.2197
			FP2	0.41282	3434.518	202.5113
			FP3	0.10567	3588.774	140.2836
	80%	Bulk	FP1	0.55129	3258.051	273.1318
			FP2	0.31291	3443.082	177.2843
			FP3	0.13013	3585.665	160.1867
		Solute-correlated	FP1	0.46186	3251.538	265.2893
			FP2	0.409	3435.592	188.7098
			FP3	0.12742	3584.677	144.2562
	100%	Bulk	FP1	0.55005	3257.609	272.6806
			FP2	0.31466	3442.956	177.5839
			FP3	0.1296	3585.751	160.0614
		Solute-correlated	FP1	0.52866	3277.869	299.9991
			FP2	0.34924	3444.578	188.2541
			FP3	0.1187	3588.317	135.1937

7. Simulation Details

As stated in the main manuscript, all simulations were performed with the LAMMPS simulation package, and all initial configurations were generated in part using inbuilt LAMMPS utilities, in combination with in-house code. All simulations were initially configured with the same idealised Au(111) slab, with all particles at their equilibrium lattice positions. To ensure meaningfully different conditions, each simulation run was initialised with a different random seed for assigning of initial velocities and initial fluid configurations.

The fluid cells were generated/equilibrated separately from the gold slab, then later merged and allowed to equilibrate further for a shorter time period. The initial fluid region configuration was sized to match the gold slab exactly in the x and y dimensions, while being significantly taller in the z direction than the final boxes, to initially give a significantly lower density (≈ 0.1 kg m^{-3}). This approach was chosen as LAMMPS uses a naïve algorithm for randomly populating particles which does not take into account the positions of already present particles, inevitably leading to simulation failures due to overlapping particles. The box was then randomly populated with citrate, water and sodium particles, and velocities assigned randomly. The initial step of equilibration was carried out using the *nvt/sllod* time integration algorithm as implemented in LAMMPS, while the size of the box was deformed to reach a more sensible density (although still somewhat low to avoid overshooting). During this process, a repulsive harmonic potential was applied at the top and bottom of the simulation boxes to facilitate later merging with the gold slab. The liquid and gold simulation cells were then merged, and the combined system allowed to further equilibrate under the NPT and NVT ensembles for a total equilibration time of 10 ns simulation time. The method of equilibration utilised for the fluid boxes inherently led to slight variation in the total height of the boxes, varying from 66.1 Å to 67.2 Å – such a small difference ensures that the results between boxes and concentrations are still comparable. The gold slab in all cases was very close to 14.1 Å thick in the z-direction (subject to very minor variation), and all boxes were enforced to be 51.9*55.0 Å in the x and y directions respectively.

No new parameters were derived for this work, instead models were selected from previous works, based on their properties and level of acceptance. The SPC/E water model[1] was chosen due to its balance of simple structure with reasonable bulk properties, and its wide use and proven track record. The citrate model and its parameters were taken from Wright *et al.* 2013,[2] which employs an approach of a flexible citrate model based on the CHARMM force field, with some modifications to better reproduce the exected properties. This model has previously been employed for the simulation of AuNPs,[3] and is compatible with the SPC/E water model. The Au model developed by Geada *et al.* 2018,[4] was chosen for two main reasons; given its drude oscillator-based approach it works very well in reproducing the electrostatic properties of gold, while also remaining a relatively straightforward model in terms of its computational efficiency, thus not limiting the size of gold slab which could be employed. In the original work, its parameters were calculated to best reproduce the expected polarizability of gold atoms, with some limits applied to ensure the model would still be usable and not restrict the simulation design too greatly. See Geada *et al.* 2018 for more details and the model parameters.

The production simulations all encompassed 40 ns simulation time under the NVT ensemble at 300 K. Frames were taken for analysis every 125 fs of simulation time and post-processed with a mix of in-house code and LAMMPS utilities. RDFs were calculated in post with LAMMPS; as were number density profiles, which were then symmetrised/averaged across all corresponding simulation boxes by way of aligning the gold planes. The tetrahedral order parameter was calculated entirely with in-house code, which binned the relevant water molecules based on the z coordinate of their oxygen atom at each time frame. For each water molecule in the region of interest, the local tetrahedral order parameter was then calculated using the method described in Duboué-Dijon and Laage, 2015.[5]

Electrostatic potential profiles were calculated for each simulation box (and then also symmetrised/averaged between multiple), primarily to validate the applicability of the simulations to the expected properties of AuNPs. Charge density profiles were calculated by summing the LAMMPS calculated per-species number density profiles with each species' respective proscribed charge. The integration to calculate the electrostatic potential was performed using the cumulative Simpson rule in accordance with the well-known Poisson's equation:

$$\varphi(z) = -\int_0^z \int_0^{z'} \frac{\rho(z)}{\varepsilon_0}\, dz''dz'$$

With a correction applied after the first integral to ensure that the bulk-like $\frac{d\varphi}{dz}$ is set to zero. The electrostatic potential was calculated per-trajectory, and then averaged across all corresponding simulation boxes using the same symmetrisation method as described for number density. It was observed that for all concentrations (including in the case of pure water), there was a potential drop between the Au surface and the bulk-like fluid region:

Table S4.

Concentration	Potential drop (mV)
0	598.8
0.1	645.6
0.25	867.0
0.5	1074.5

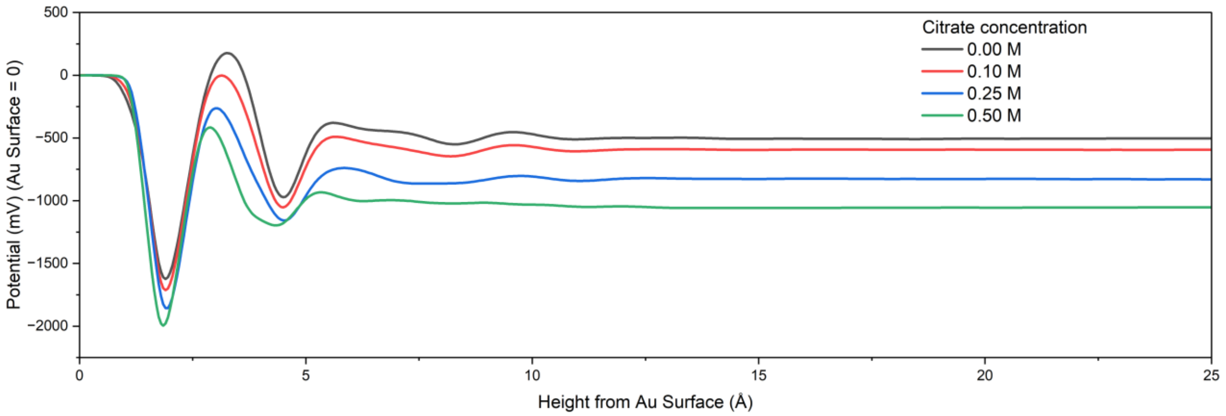

Figure S3. Average electrostatic potential in the z-direction relative to the Au surface. Values are shifted so that the potential at the Au surface is 0 for ease of comparison. A clear drop is present in the potential, enhanced with increasing sodium citrate concentration but also present with pure water, likely due to alignment between the water dipoles.

This observed potential drop is consistent with the accepted potential drop observed at the AuNP interface, whereby the nanoparticles are stabilised by the presence of a mutually repulsive electrostatic potential.

8. Citrate Aggregation in the Simulations

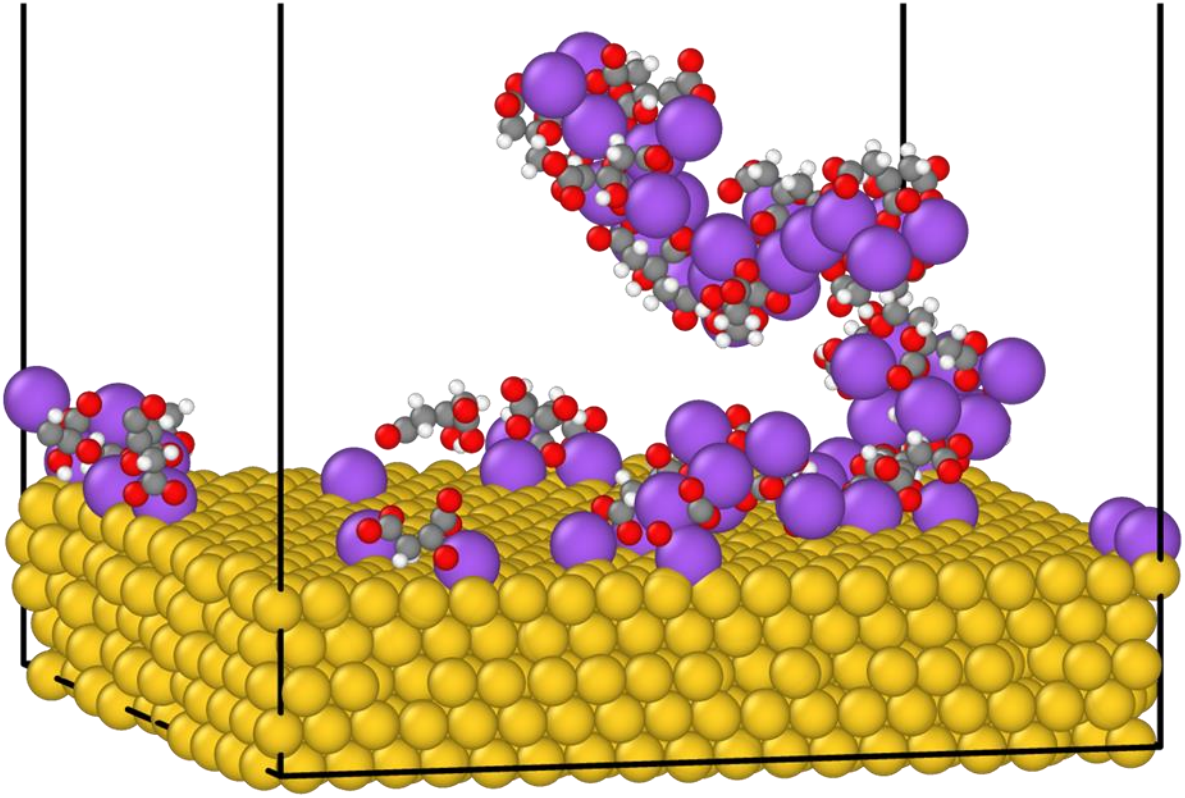

Figure S4. A characteristic snapshot from a simulation trajectory, with explicit SPC/E water removed for visual clarity. Consistent with previous simulation-based works, a fraction of the sodium and citrate ions were observed to adsorb closely to the Au interface, while others formed relatively long agglomerates. This behaviour was observed at all concentrations and in every case a significant portion of the sodium and citrate adsorbed directly to the interface, while the observed agglomerates also tended to interact with the surface closely.

9. Interfacial Density Profile and Radial Distribution Function

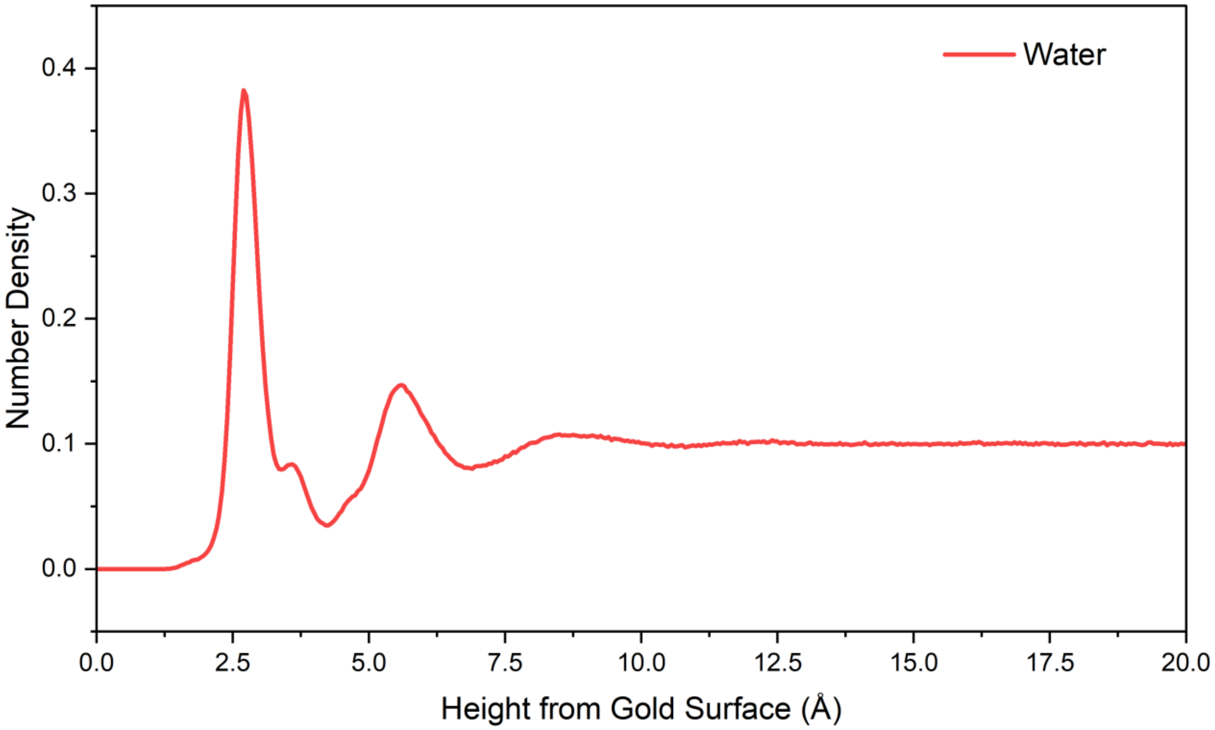

Figure S5. Interfacial number density profile of water above the Au(111) surface, in a selected simulation of 0.25 M sodium citrate solution. The important feature to note is the length scale of the increase in density from the surface, which extend to ~10 Å from the Au surface.

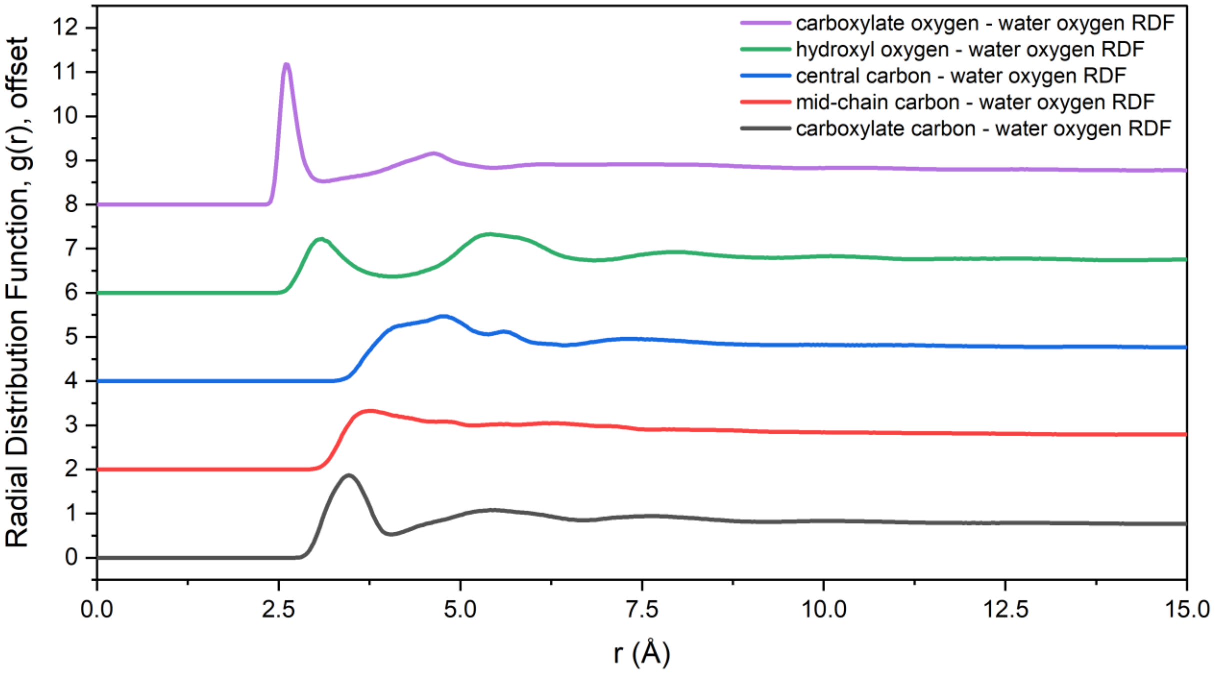

Figure S6. Radial distribution functions of the water oxygens from various sites in the citrate molecules. It is clear that both the carboxylate and hydroxyl oxygens of the citrate engage hydrophilically with the water.

10. Choice of citrate concentration in the simulation

One complicating factor affecting the analyses of the simulation results is the choice of an appropriate sodium citrate concentration for applicability to the interfacial region. In general, computational studies report[3] that citrate adsorbs to the gold surface and forms aggregate-like chains, which was also observed in these simulations (see **Figure S4**), leading to a higher effective concentration directly in the interfacial region than in the solution as a whole. Given that the citrate concentrations in the AuNP samples used for the experiments (see SI sections 1 and 2), were all well below the concentrations used in the simulations, it is understood that the influence of citrate concentration gradient on the extent of the deviation of water structure from tetrahedrality, in the real samples should be even less prominent than in the models used for the simulations.

11. Potential influence of temperature fluctuation

An excitation wavelength of around 515 nm was employed in this work. This wavelength is very close to the surface plasmon resonance peaks of all the Au NP samples, which makes it obvious that a heating of the samples due to greater photon absorption cannot be avoided during the Raman spectral measurements. If a possible local heating around Au NPs cannot be dispersed off by the use of thermal regulation applied in the current work, the local heating could lead to an increased temperature of the solvation shell compared to the bulk. In such a scenario, one cannot rule out the implication that the differences between solute-correlated and bulk Raman spectra could primarily have been the results of comparing the spectra of essentially identical aqueous samples that were merely recorded at different temperatures. Here, the goal for this control experiment was to examine the effect of heating on the Raman spectral lineshapes of water and to assert if similar spectral changes were observed in case of the experiments with NP samples and their corresponding dispersing media.

In order to note the differences in spectral profiles amongst the various samples in every set, followed by an identical data processing workflow (baseline subtraction followed by area normalisation as described in the 'Methods'), the first spectrum in the water spectra series was subtracted from the rest of the spectra for this blank experiment. Similarly, in case of NP10, NP30 and NP50 series, for every pair of NP sample and their corresponding dispersing medium (bulk), the latter was subtracted from the former. These difference spectra were compared against those for the blank experiment.

It was found that the difference spectra for the blank experiment (**Figure S7**) show features largely distinct from the ones for the NP10, NP30 and NP50 series (**Figure S8**). The difference spectra for the 20% data have some degree of similarity with the difference spectra from the temperature increment experiment but the rest do not show any similarity at all. If the changes were similar, subjecting a pair of water spectra measured at two different temperatures, to MCR, could lead to similar purported 'solute-correlated' spectra since, in a 2-component MCR, every spectral feature of the mixture spectrum that is different than the pure bulk spectrum, shows up in the solute-correlated spectrum. Therefore, it can safely be concluded that the solute-correlated spectra reported in this article, are not merely due to local temperature fluctuations, even if they occur.

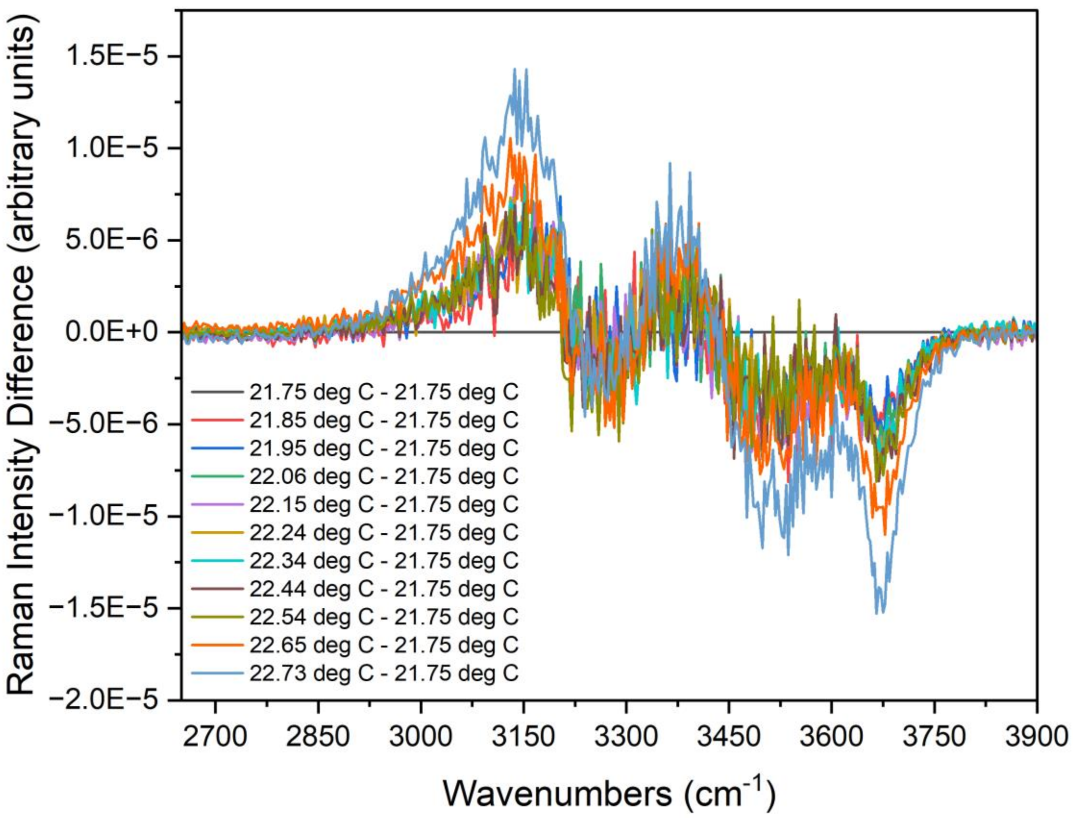

Figure S7. Raman difference spectra for water spectra recorded at increasing temperatures. The first spectrum in the series was subtracted from each one of them.

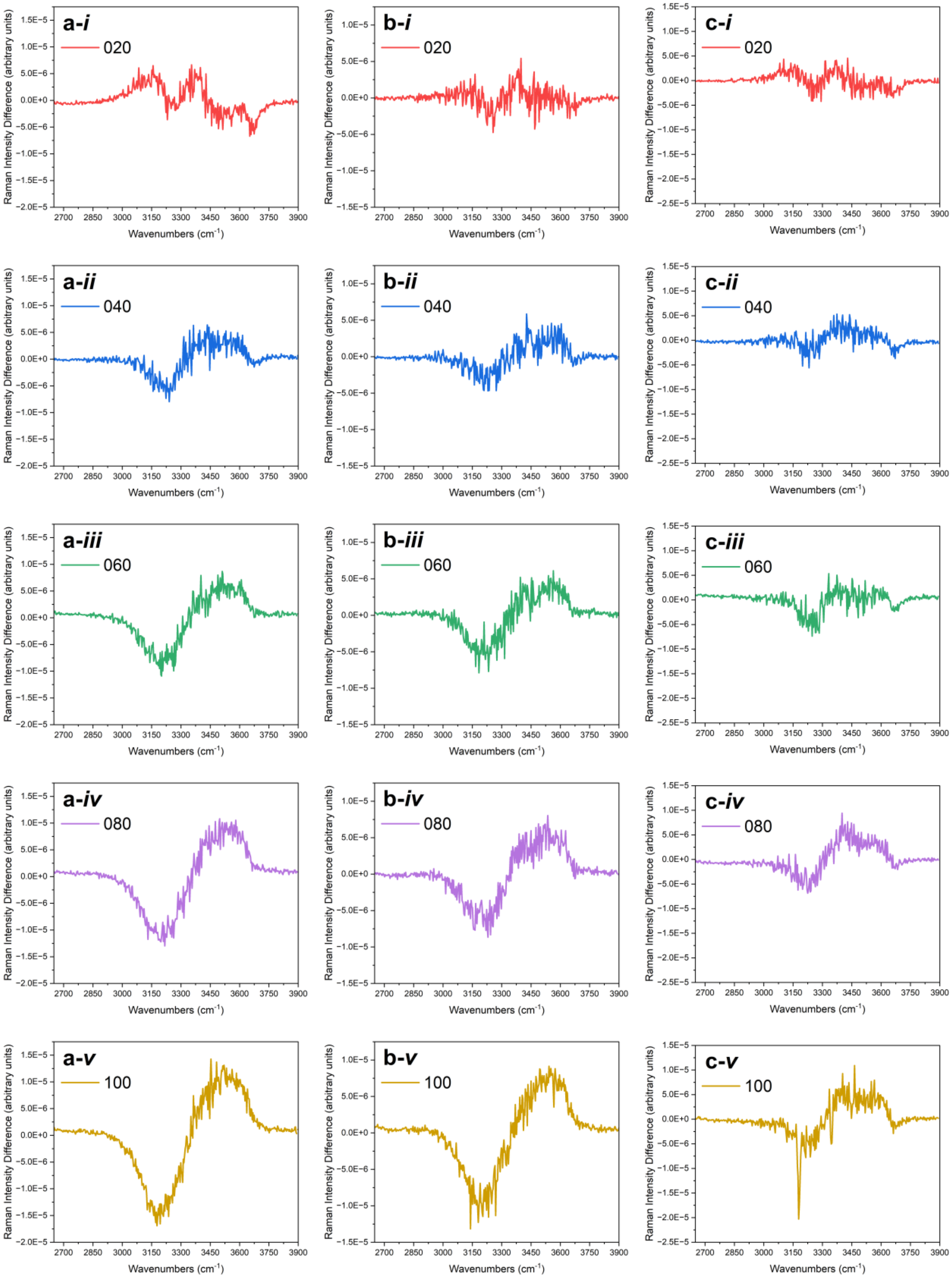
a-i
020
b-i
020
c-i
020
a-ii
040
b-ii
040
c-ii
040
a-iii
060
b-iii
060
c-iii
060
a-iv
080
b-iv
080
c-iv
080
a-v
100
b-v
100
c-v
100
Raman Intensity Difference (arbitrary units)
Wavenumbers (cm^{-1})
2700
2850
3000
3150
3300
3450
3600
3750
3900
1.5E−5
1.0E−5
5.0E−6
0.0E+0
−5.0E−6
−1.0E−5
−1.5E−5
−2.0E−5
−2.5E−5

Figure S8. Raman difference spectra obtained by subtracting the bulk spectrum from the solute-correlated spectrum for (*i*) 20%, (*ii*) 40%, (*iii*) 60%, (*iv*) 80%, (*v*) 100% samples in the a. NP10, b. NP30 and c. NP50 series.

References

1 H. J. C. Berendsen, J. R. Grigera and T. P. Straatsma, *J. Phys. Chem.*, 1987, **91**, 6269–6271.
2 L. B. Wright, P. M. Rodger and T. R. Walsh, *RSC Adv.*, 2013, **3**, 16399–16409.
3 O. A. Perfilieva, D. V. Pyshnyi and A. A. Lomzov, *J. Chem. Theory Comput.*, 2019, **15**, 1278–1292.
4 I. L. Geada, H. Ramezani-Dakhel, T. Jamil, M. Sulpizi and H. Heinz, *Nat. Commun.*, 2018, **9**, 716.
5 E. Duboué-Dijon and D. Laage, *J. Phys. Chem. B*, 2015, **119**, 8406–8418.